Aalborg Universitet

AALBORG UNIVERSITY

Active Power Oscillation Damping Based on Acceleration Control in Paralleled Virtual Synchronous Generators System

Chen, Meng; Zhou, Dao; Blaabjerg, Frede

Published in:
I E E E Transactions on Power Electronics

DOI (link to publication from Publisher):
10.1109/TPEL.2021.3051272

Publication date:
2021

Document Version
Accepted author manuscript, peer reviewed version

Link to publication from Aalborg University

Citation for published version (APA):
Chen, M., Zhou, D., & Blaabjerg, F. (2021). Active Power Oscillation Damping Based on Acceleration Control in Paralleled Virtual Synchronous Generators System. *I E E E Transactions on Power Electronics*, *36*(8), 9501-9510. Article 9321738. https://doi.org/10.1109/TPEL.2021.3051272

General rights
Copyright and moral rights for the publications made accessible in the public portal are retained by the authors and/or other copyright owners and it is a condition of accessing publications that users recognise and abide by the legal requirements associated with these rights.

- Users may download and print one copy of any publication from the public portal for the purpose of private study or research.
- You may not further distribute the material or use it for any profit-making activity or commercial gain
- You may freely distribute the URL identifying the publication in the public portal -

Take down policy
If you believe that this document breaches copyright please contact us at vbn@aub.aau.dk providing details, and we will remove access to the work immediately and investigate your claim.

Downloaded from vbn.aau.dk on: December 06, 2025

Active Power Oscillation Damping Based on Acceleration Control in Paralleled Virtual Synchronous Generators System

Meng Chen, *Student Member, IEEE,* Dao Zhou, *Senior Member, IEEE,* and Frede Blaabjerg, *Fellow, IEEE*

***Abstract*—Although the virtual synchronous generator provides a grid-friendly operational mode for power converters, it may also introduce disadvantages similar with a traditional synchronous generator such as power oscillation in the parallel mode due to a large virtual inertia. This paper proposes an additional damping strategy to suppress the power oscillation. After analyzing the relationship between the output power and the angular acceleration, a damping strategy is designed by the acceleration control with a disturbance compensation. Small-signal analysis is also applied to study the stability of the proposed method. Finally, experiments are carried out to verify the proposed auxiliary damping method.**

***Index Terms*—Virtual synchronous generator, parallel operation, damping control, power oscillation, acceleration control.**

I. Introduction

MOTIVATED by the favorable characteristics of a traditional synchronous generator, the virtual synchronous generator (VSG) is proposed in order to overcome the shortages of the common control strategies applied in an inverter, which are lacking of inertia in general [1]–[6]. By applying the mathematical model of a synchronous generator in the control system, an inverter can emulate the inertia characteristics even though there is not an actual mechanical rotor [7], [8]. Therefore, the frequency performance will be improved in a power system with more power-electronic-based power supplies using the virtual inertia. In the case of a system without inertial sources such as some islanded microgrids, this feature is especially important.

Plenty of implementations have been proposed for the VSG [9], [10]. Although there are different modeling approaches among them, the key characteristic of inertia is always introduced by imitating the swing equation of the rotor in a synchronous generator. Simultaneously, in this way, the synchronization is naturally changed to a power-based process rather than depending on a phase-locked loop (PLL). In addition, the steady-state droop characteristics of the governor and the automatic voltage regulator (AVR) in a synchronous generator can easily be applied to a VSG as well. Currently, there is no standard on how the transient response of a VSG should be. However, as synchronous generators have been well used in the power system, which shows good robustness, it could be a good way to control a VSG to behave as close as possible to a synchronous generator. An improved implementation motivated by this point is proposed in [11]. In conclusion, from the viewpoint of the power grid, a static inverter can operate in the way of a rotating synchronous generator [12]. Therefore, the VSG is seen as a grid-friendly way to integrate the power-electronic-based sources without threatening the normal operation of the traditional power grid.

Nevertheless, some disadvantages of a synchronous generator may still be observed in a VSG, one of which is the power oscillations due to the large inertia [13], [14]. In parallel VSG systems, this phenomenon can easier occur [15]–[18]. Compared to an actual synchronous generator, the power oscillation may have more serious impacts on a VSG. This is because the power semiconductor devices have lower overcurrent capability and the damping of a power-electronic-based grid is much smaller.

In [17], the center of inertia is used to damp the power oscillation in a paralleled VSGs system. However, it has to depend on a central controller. In some decentralized implementations, the damping of a VSG can be improved by adding a PLL-based virtual damping term. This will inevitably introduce PLL-related problems, especially in a weak grid [19]. Similarly, the droop control can be used to improve the damping ability [20], [21]. However, it is most preferable in the case of the grid-connected mode. In an islanded system with parallel VSGs, changing the droop control will influence the steady-state regulation characteristics. In [22], a non-linear power damping controller is proposed. However, the coupling between the frequency and voltage control is increased. Meanwhile, the analysis of a non-linear system is difficult. In comparison, a linear damping control strategy for a VSG is presented in [23]. Nevertheless, it focuses on the oscillations caused by the coupling between the active and reactive power control loops, and the parameters are determined by a complicated online algorithm. Some easier online damping correction methods can be found in [24]–[26], which are designed by self-adaptive or optimal control. All these methods are based on a stiff power grid, which may not be applied when the steady-state frequency of the system changes in an islanded system. In [27], a damping correction loop is used in order to increase the degree of freedom of a single synchronverter, where damping the power oscillations in a parallel system is not considered. Virtual impedance is another effective method to improve the stability of a single VSG [28], [29]. As described in [30] and [31], the power oscillation for parallel VSGs can be canceled when there are specific relationships between parameters of the VSGs including the virtual impedances. This requires a

The authors are with the Department of Energy Technology, Aalborg University, Denmark (e-mail: mche@et.aau.dk; zda@et.aau.dk; fbl@et.aau.dk).

central manage to design the parameters of all parallel VSGs simultaneously, which is inflexible and may not be feasible in practice. Meanwhile, even though the virtual impedances can be designed properly, the performance can still be influenced by the impedances of the lines, whose accurate values are difficult to be obtained. Although a damping strategy proposed in [31] helps to decrease the power oscillation, it shows that a large oscillatory magnitude can still be observed without a proper impedance matching.

This paper focuses on providing a damping strategy to suppress the power oscillation for parallel VSGs with only the locally available information. Although the parameters of the parallel VSGs do not meet a specific requirement, the power oscillation can still be well damped by using the proposed method.

The rest of the paper is organized as follows. Section II provides a brief introduction of the VSG and power oscillation in the parallel mode. In Section III, the proposed additional damping method based on the acceleration control is described in details, and the stability analysis is given in Section IV. Section V presents the experimental results. Finally, the conclusions are drawn in Section VI.

II. Active Power Oscillation of Parallel VSGs

A. Overview of Conventional VSG

Fig. 1 shows the topology and the control block diagram of a traditional VSG. The power stage consists of a DC source represented by V_{dc}, and a three-phase inverter with an LC filter, where L_f, R_f, and C_f are the equivalent inductance and resistance of the filter inductor, and the filter capacitance. L_s and R_s represent the equivalent inductance and resistance connecting to a main grid, microgrid, or just a local load according to different operation modes. i, v, and i_o are the currents of the filter inductor, the output voltages, and the output currents, respectively. The subscripts "abc" and "dq" represent the components in the abc and dq frames. The output active power p and reactive power q are calculated and fed into the VSG control to derive the voltage references v_{dqref} for the inner voltage and current control loops. In this paper, if there is not specific illustration, all the following modeling and analysis are given based on the p.u. system.

The VSG control emulates the characteristics and control of an actual synchronous generator, which consists of four parts, i.e., the virtual rotor, virtual winding, virtual governor and virtual AVR. The virtual rotor represents the inertia characteristics, which is expressed as

$$\begin{cases} P_0 - p^* - p_d = 2H\dfrac{d\omega^*}{dt} \\ \dfrac{d\theta}{dt} = \omega^*\omega_n \end{cases} \tag{1}$$

where the superscript "*" represents the p.u. value and the subscript "0" represents the set-point value. p_d is the damping power, ω and ω_n are the virtual angle speed of the rotor and its nominal value, and θ is the rotor angle. H is the inertia constant. The virtual winding represents the electromagnetic characteristics, which uses the steady-state model to enhance

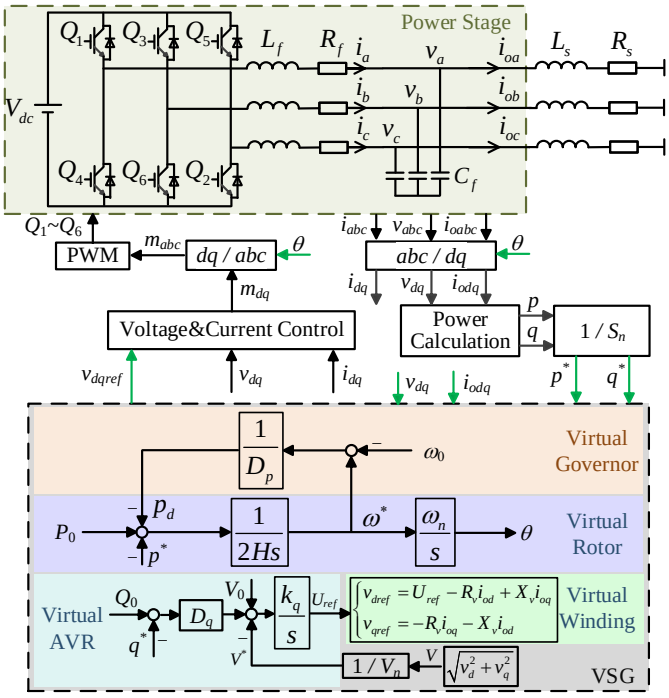

Fig. 1. Topology and control structure of a traditional VSG.

the decoupling of the influence between the active and reactive power.

The virtual governor and virtual AVR emulate the frequency and voltage regulation in the traditional power system by using droop control, which can be expressed as

$$-D_p p_d = \omega_0 - \omega^* \tag{2}$$

$$U_{ref} = k_q \int [D_q(Q_0 - q^*) + V_0 - V^*]dt \tag{3}$$

where D_p and D_q are the $P-\omega$ and $Q-V$ droop coefficients. As seen from Fig. 1, the feedback signal of voltage magnitude V and the angle for coordinate transformation are obtained from the control signals, which implies that the PLL can be completely eliminated.

B. Causes of Active Power Oscillation

When voltage sources such as VSGs are paralleled with each other, the power oscillation may occur due to the re-synchronization process after a disturbance. The system used in this paper is shown in Fig. 2, which includes two VSGs as an example.

According to Fig. 1, the state-space representation of the frequency regulation following a load disturbance can be expressed as [30]

$$\begin{cases} \dot{\boldsymbol{x}} = \boldsymbol{A}\boldsymbol{x} + \boldsymbol{B}\Delta p^*_{load} \\ \boldsymbol{y} = \boldsymbol{C}\boldsymbol{x} + \boldsymbol{D}\Delta p^*_{load} \end{cases} \tag{4}$$

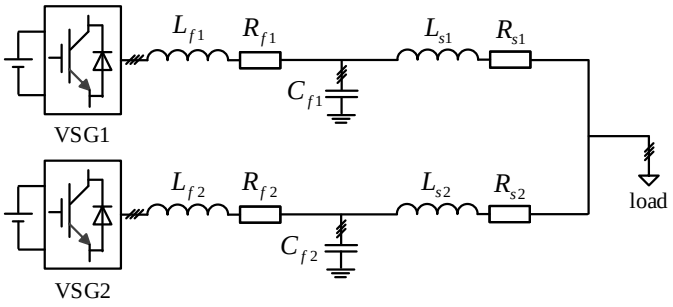

Fig. 2. Topology of two paralleled VSG systems connected to a load.

where

$$\boldsymbol{x} = \begin{bmatrix} \Delta\dot{\omega}_1^* & \Delta\dot{\omega}_2^* & \Delta\delta \end{bmatrix}^T \tag{5}$$

$$\boldsymbol{y} = \begin{bmatrix} \Delta p_1^* & \Delta p_2^* \end{bmatrix}^T \tag{6}$$

$$\boldsymbol{A} = \begin{bmatrix} -\frac{1}{2H_1 D_{p1}} & 0 & -\frac{K_1 K_2}{2H_1(K_1+K_2)} \\ 0 & -\frac{1}{2H_2 D_{p2}} & \frac{K_1 K_2}{2H_2(K_1+K_2)} \\ \omega_n & -\omega_n & 0 \end{bmatrix} \tag{7}$$

$$\boldsymbol{B} = \begin{bmatrix} -\frac{K_1}{2H_1(K_1+K_2)} & -\frac{K_2}{2H_2(K_1+K_2)} & 0 \end{bmatrix}^T \tag{8}$$

$$\boldsymbol{C} = \begin{bmatrix} 0 & 0 & \frac{K_1 K_2}{K_1+K_2} \\ 0 & 0 & -\frac{K_1 K_2}{K_1+K_2} \end{bmatrix} \tag{9}$$

$$\boldsymbol{D} = \begin{bmatrix} \frac{K_1}{K_1+K_2} & \frac{K_2}{K_1+K_2} \end{bmatrix}^T \tag{10}$$

where K_1 and K_2 are two parameters determined by the steady-state operation point calculated by

$$K_i = \left.\frac{\partial p_i}{\partial \delta_i}\right|_{\infty} \tag{11}$$

and i is 1 or 2 for VSG1 and VSG2, respectively. As seen, the paralleled VSGs are interconnected with each other by the relative rotor angle $\Delta\delta$=$\Delta\theta_1 - \Delta\theta_2$. According to the loci analysis in [31], the state variable of $\Delta\delta$ may introduce a pair of conjugate plural dominated poles, which leads to oscillations in the output power.

III. Proposed Damping Control

A. Analysis of Control Target and Control Signal

Based on (1) and (2), the frequency dynamics of the VSG can be represented as

$$P_0 + \frac{1}{D_p}(\omega_0 - \omega^*) - p^* = 2H\frac{d\omega^*}{dt} \tag{12}$$

In order to damp the power oscillation, a new control input u is added in (12) as

$$u + P_0 + \frac{1}{D_p}(\omega_0 - \omega^*) - p^* = 2H\frac{d\omega^*}{dt} \tag{13}$$

By rearranging (13), the output power of the VSG can be expressed as

$$p^* = u + P_0 + \frac{1}{D_p}\omega_0 - \frac{1}{D_p}\omega_\infty^* - (\frac{1}{D_p}\int\frac{d\omega^*}{dt}dt + 2H\frac{d\omega^*}{dt}) \tag{14}$$

where ω_∞^* is the initial value. As shown, the VSG can be seen as a system, where the output p^* is controlled by $d\omega^*/dt$ via a PI controller with proportional and integral gains being $2H$ and $1/D_p$, respectively. Neglecting the effect of the constant term $P_0 + (1/D_p)\omega_0 - (1/D_p)\omega_\infty^*$, p^* is expressed in the frequency domain as

$$p^*(s) = u(s) - \frac{2Hs + 1/D_p}{s}\dot{\omega}^*(s) \tag{15}$$

Therefore, the oscillatory characteristics of $p^*(s)$ is determined by the poles of $\dot{\omega}^*(s)$ and $u(s)$. If $\dot{\omega}^*(s)$ and $u(s)$ introduce conjugate plural dominated poles, oscillations will occur in the output active power. Otherwise, if $\dot{\omega}^*(s)$ and u can only introduce negative real poles, no oscillations will be observed in the output power.

According to the aforementioned analysis, it is possible to control the output power by the controlling of $d\omega^*/dt$. If the dynamics of $d\omega^*/dt$ can be damped with a damped input u, no oscillations will occur in p^*. Besides, the P-ω droop characteristics in the steady-state should not be changed in order to keep an accurate power sharing among VSGs, which requires that, according to (13), the steady-state value of the control input u is zero. In summary, the control targets can be expressed as follows.

1) Poles of $\dot{\omega}^*(s)$ are negative real poles.
2) Poles of u are negative real poles.
3) $\lim_{t\to\infty} u = 0$

B. Acceleration Control Based damping control

Based on Section III-A, the power oscillation can be controlled by the angular acceleration $\dot{\omega}^*$. By choosing $\dot{\omega}^*$ as a state variable, the time derivative of (13) is

$$\dot{u} - \frac{1}{D_p}\dot{\omega}^* - \dot{p}^* = 2H\ddot{\omega}^* \tag{16}$$

As the control input u itself should be controlled as well, u is seen as the second state space. By defining an intermediate variable μ as

$$\dot{u} = \mu \tag{17}$$

the state-space representation of acceleration control of the VSG can be expressed as

$$\begin{bmatrix} \ddot{\omega}^* \\ \dot{u} \end{bmatrix} = \begin{bmatrix} -\frac{1}{2HD_p} & 0 \\ 0 & 0 \end{bmatrix}\begin{bmatrix} \dot{\omega}^* \\ u \end{bmatrix} + \begin{bmatrix} \frac{1}{2H} \\ 1 \end{bmatrix}\mu + \begin{bmatrix} -\frac{1}{2H} \\ 0 \end{bmatrix}\dot{p}^* \tag{18}$$

$$\begin{bmatrix} \dot{\omega}^* \\ u \end{bmatrix} = \begin{bmatrix} 1 & 0 \\ 0 & 1 \end{bmatrix}\begin{bmatrix} \dot{\omega}^* \\ u \end{bmatrix} \tag{19}$$

As seen, the model is a single input, double output system and there is a disturbance introduced by $\dot{p}^*$. It should be mentioned that the so-called disturbance is an equivalent term in mathematics but not representing the actual disturbance of the system. As seen in the equivalent circuit of the paralleled VSGs system shown in Fig. 3, the actual disturbance for VSG 1 comes from the rest parts of the system such as the load variation, the output of VSG 2, etc. However, all these disturbances will be reflected in the variation of p_1^*. Therefore, $\dot{p}^*$ includes the information of the actual disturbances, which is used to design the controller according to (18).

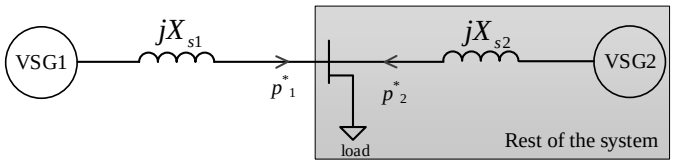

Fig. 3. Equivalent circuit diagram of paralleled VSGs system.

Firstly, if neglecting the disturbance, the dynamics of the outputs are expected to be completely controlled by the state feedback control. However, the disturbance may influence the performance of the controller. In order to decrease the impact of $\dot{p}^*$, a large control gain should be used. In the following stability analysis, it will show that instability may occur in this case by leading one of the negative real root to cross the imaginary axis. This is because the disturbance matrix $\boldsymbol{B_d}$ is not adjustable by the feedback control. The virtual impedances are used to avoid using a large feedback gain [31]. However, as stated above, the impedances of the parallel VSGs may not exactly meet the required relationship.

It is worth noting that the disturbance $\dot{p}^*$ will return to be zero in steady-state. Therefore, in order to take the disturbance into consideration in the feedback control, take $\dot{p}^*$ as the third state variable. Then the state-space representation of (18) and (19) are extended to the following

$$\begin{bmatrix} \dot{\omega}^* \\ \dot{u} \\ \ddot{p}^* \end{bmatrix} = \begin{bmatrix} -\frac{1}{2HD_p} & 0 & -\frac{1}{2H} \\ 0 & 0 & 0 \\ 0 & 0 & 0 \end{bmatrix} \begin{bmatrix} \dot{\omega}^* \\ u \\ \dot{p}^* \end{bmatrix} + \begin{bmatrix} \frac{1}{2H} \\ 1 \\ 0 \end{bmatrix} \mu + \begin{bmatrix} 0 \\ 0 \\ 1 \end{bmatrix} \ddot{p}^* \tag{20}$$

$$\begin{bmatrix} \dot{\omega}^* \\ u \end{bmatrix} = \begin{bmatrix} 1 & 0 & 0 \\ 0 & 1 & 0 \end{bmatrix} \begin{bmatrix} \dot{\omega}^* \\ u \\ \dot{p}^* \end{bmatrix} \tag{21}$$

Compared the upper model with a standard state space model, $\begin{bmatrix} \dot{\omega}^* & u & \dot{p}^* \end{bmatrix}^T$ can be seen as the state vector and μ can be seen as the input. Then according to the state feedback theory, the control signal μ can be defined as [32]

$$\mu = -\begin{bmatrix} k_1 & k_2 & k_3 \end{bmatrix} \begin{bmatrix} \dot{\omega}^* & u & \dot{p}^* \end{bmatrix}^T \tag{22}$$

where k_1, k_2, k_3 are the feedback gains. Combining (17) and (22) yields

$$\dot{u} = -\begin{bmatrix} k_1 & k_2 & k_3 \end{bmatrix} \begin{bmatrix} \dot{\omega}^* & u & \dot{p}^* \end{bmatrix}^T = -k_1\dot{\omega}^* - k_2 u - k_3\dot{p}^* \tag{23}$$

Then u can be solved in the s domain as

$$u = -\frac{k_1}{s+k_2}\dot{\omega}^* - \frac{k_3 s}{s+k_2}p^* \tag{24}$$

where a more general form is

$$u = -\frac{k_1}{s+k_2}\dot{\omega}^* - \frac{k_3 s}{s+k_4}p^* \tag{25}$$

As seen, the feedback signal is a combination of the low frequency component of the frequency acceleration and the high frequency component of the active power. It should be noted that (20) is still not a standard state-space representation due to $\ddot{p}^*$. In theory, the state-space representation can be further extended by taking $\ddot{p}^*$ as a state variable in order to decrease the influence of the disturbance. However, more extended state variables will lead to more differential terms, which cannot be fulfilled in practice. The block diagram of the frequency control of the VSG with the proposed damping control strategy is shown in Fig. 4.

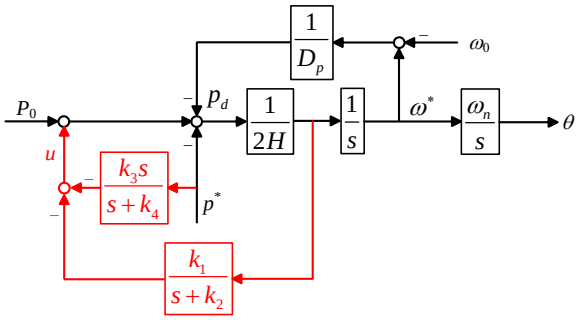

Fig. 4. Frequency control of VSG with the proposed damping method.

By choosing different feedback gains, different control performances can be achieved. The following gives a remark on some special cases.

1) Case 1: $k_1 = k_3 = 0$. It is the traditional VSG control.
2) Case 2: $k_1 = 0$. The feedback signal contains only the power signal, which is seen as a disturbance suppression control. However, $\dot{\omega}^*$ is not controlled, which implies that a large frequency deviation may occur.
3) Case 3: $k_3 = 0$. The feedback signal contains only the frequency signal. Compared with the method in [31], if setting the feedback gains as $k_1 = D$ and $k_2 = 1/T_\omega$, they are equivalent. Therefore, the damping strategy proposed in [31] can be seen as a special case of the acceleration control method in this paper. Obviously, because there is no disturbance suppression, the control performance is highly affected.
4) Case 4: $k_2 = 0$ or $k_4 = 0$. In this case, u is not controlled and the system represented by (18) and (19) is simplified to a single input, single output system. It is possible that the disturbance can be completely compensated by an active disturbance suppression in theory. However, the steady-state characteristics will inevitably be changed. Therefore, k_2 and k_4 should be compromisely chosen between better oscillation suppression and smaller steady-state error.

Based on the proposed control strategy, the closed-loop bode diagrams of $\Delta p_1^*(s)/\Delta p_{load}^*(s)$ in the parallel VSGs system shown in Fig. 2 are compared in Fig. 5. In this paper, the used parameters are the same as in the experiments shown in Section IV if there is not specific illustration. As seen, under the traditional VSG control, there will be a resonance peak at the frequency around 2.6 Hz. In Case 2, when only the disturbance suppression signal is introduced in the feedback control, the resonance is damped. However, a new resonance point occurs at a higher frequency around 10 Hz. Although this resonance can quickly be damped, a large oscillation is anticipated to be observed in the beginning of the disturbance. On the contrary, in Case 3 with only the acceleration feedback without a disturbance suppression, a smaller resonance

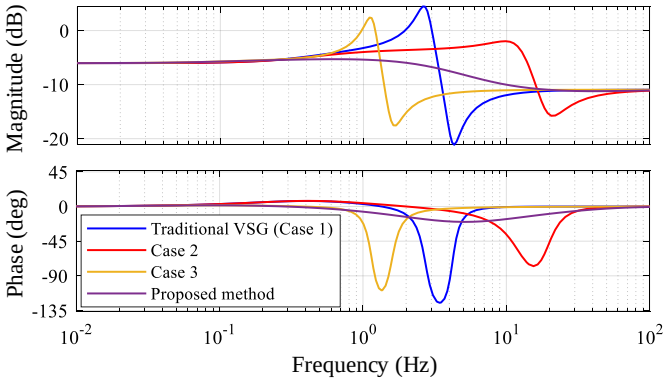

Fig. 5. Comparison of frequency characteristics with different control strategies.

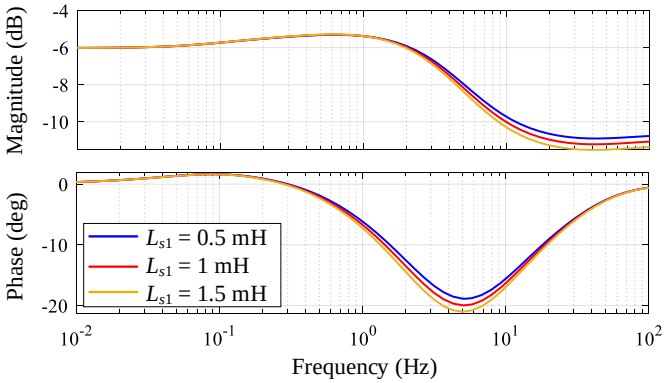

Fig. 6. Bode diagram of $\Delta p_1^*(s)/\Delta p_{load}^*(s)$ with different line impedances.

frequency around 1.1 Hz will occur. The resonance peak decreases in this situation, but a longer settle time may be needed. This is the reason why a additional virtual impedance design should be used to further damp the oscillation in [31]. With the proposed method, the existing resonance can be well damped. Meanwhile, no new resonance point with a high peak will be introduced into the system.

Before investigating the impact of the proposed controller on the stability of the system, a study on the line impedance effects is firstly carried on. As shown in the equivalent circuit of the paralleled VSGs system in Fig. 3, X_s represents the line impedance. Thanks to the function of the virtual inductor, the line can be seen as inductive. In the following, the impact of the line impedance X_{s1} will be studied. It is supposed that L_{s1} changes within $\pm 50\%$ of the used value in the experiment (1 mH). Fig. 6 shows the frequency characteristics of the system with different line impedances controlled by the proposed method. It is noted that, the low-frequency domain is hardly influenced by L_{s1}, while the gain, in a relatively high-frequency domain, decreases with the increasing of L_{s1}, which implies a larger damping. It is worth noting that the resonance peak is always damped with different line impedances compared with the traditional VSG shown in Fig. 5. Therefore, the proposed method is robust to the line impedance.

It should be mentioned that although a simple paralleled VSGs system is used in this paper, the topology of the rest of

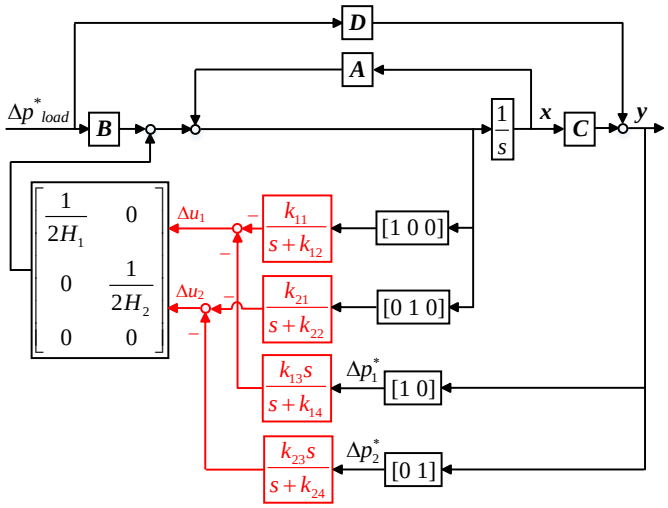

Fig. 7. Block diagram of small-signal model for parallelled VSG system.

the system in Fig. 3 can be other complicated structure with multiple VSGs. On one hand, the model can be easily derived based on the method in [33]. On the other hand, the proposed method has a relatively high robustness. It is because, as stated before in Fig. 3, all of the disturbances from the rest of the system will be reflected in the variation of p_1^* and then the control input by the designed power feedback.

C. Stability Analysis

With the proposed controllers, the dynamics of the paralleled VSG system shown in Fig. 2 is described by (4), (13), and (25). Therefore, the block diagram of the small-signal model can be derived as shown in Fig. 7. Based on this, the new state-space representation becomes,

$$\begin{cases} \dot{\boldsymbol{x}}_{new} = \boldsymbol{A}_{new}\boldsymbol{x}_{new} + \boldsymbol{B}_{new}\Delta p_{load}^* \\ \boldsymbol{y} = \boldsymbol{C}_{new}\boldsymbol{x}_{new} + \boldsymbol{D}\Delta p_{load}^* \end{cases} \tag{26}$$

where a new state vector $\boldsymbol{x}_{new}$ is

$$\boldsymbol{x}_{new} = \begin{bmatrix} \boldsymbol{x} & x_1 & x_2 & x_3 & x_4 \end{bmatrix}^T \tag{27}$$

where x_1 and x_2 are the new state variables introduced by the proposed feedback controllers in VSG1, and x_3 and x_4 are the new state variables in VSG2. In addition, the state transition matrix is shown in (30) (on top of the next page), and the other matrices are given as

$$\boldsymbol{B}_{new} = \begin{bmatrix} \boldsymbol{B} - \begin{bmatrix} \frac{k_{13}}{2H_1} & 0 \\ 0 & \frac{k_{23}}{2H_2} \\ 0 & 0 \end{bmatrix} \boldsymbol{D} \\ \begin{bmatrix} 0 & 0 & 0 \\ k_{11} & 0 & 0 \\ 0 & 0 & 0 \\ 0 & k_{21} & 0 \end{bmatrix} \boldsymbol{B} + \begin{bmatrix} k_{13}k_{14} & 0 \\ -\frac{k_{11}k_{13}}{2H_1} & 0 \\ 0 & k_{23}k_{24} \\ 0 & -\frac{k_{21}k_{23}}{2H_2} \end{bmatrix} \boldsymbol{D} \end{bmatrix} \tag{28}$$

$$\boldsymbol{C}_{new} = \boldsymbol{C} \begin{bmatrix} 1 & 0 & 0 & 0 & 0 & 0 & 0 \\ 0 & 1 & 0 & 0 & 0 & 0 & 0 \\ 0 & 0 & 1 & 0 & 0 & 0 & 0 \end{bmatrix} \tag{29}$$

$$\boldsymbol{A}_{new} = \begin{bmatrix} \boldsymbol{A} - \begin{bmatrix} \frac{k_{13}}{2H_1} & 0 \\ 0 & \frac{k_{23}}{2H_2} \\ 0 & 0 \end{bmatrix} \boldsymbol{C} & \begin{bmatrix} \frac{1}{2H_1} & -\frac{1}{2H_1} & 0 & 0 \\ 0 & 0 & \frac{1}{2H_2} & -\frac{1}{2H_2} \\ 0 & 0 & 0 & 0 \end{bmatrix} \\ \begin{bmatrix} 0 & 0 & 0 \\ k_{11} & 0 & 0 \\ 0 & 0 & 0 \\ 0 & k_{21} & 0 \end{bmatrix} \boldsymbol{A} + \begin{bmatrix} k_{13}k_{14} & 0 \\ -\frac{k_{11}k_{13}}{2H_1} & 0 \\ 0 & k_{23}k_{24} \\ 0 & -\frac{k_{21}k_{23}}{2H_2} \end{bmatrix} \boldsymbol{C} & \begin{bmatrix} -k_{14} & 0 & 0 & 0 \\ \frac{k_{11}}{2H_1} & -k_{12} - \frac{k_{11}}{2H_1} & 0 & 0 \\ 0 & 0 & -k_{24} & 0 \\ 0 & 0 & \frac{k_{21}}{2H_2} & -k_{22} - \frac{k_{21}}{2H_2} \end{bmatrix} \end{bmatrix} \tag{30}$$

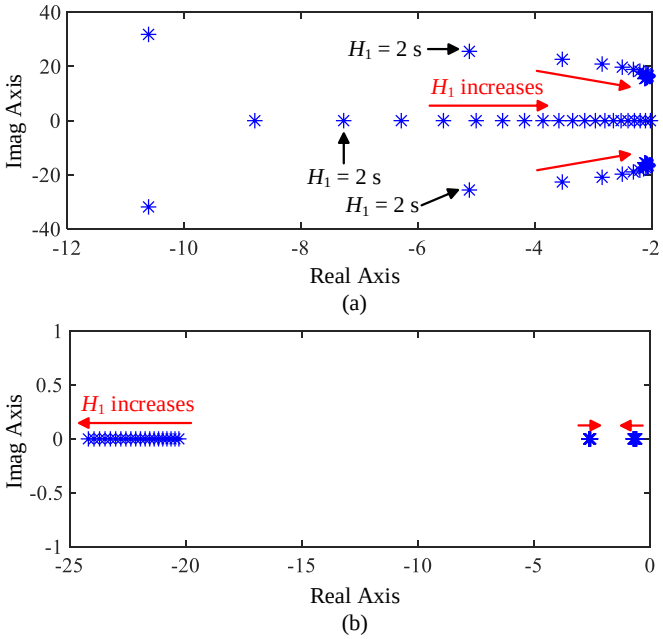

Fig. 8. Dominated poles when H_1 increases from 1 s to 20 s of (a) traditional VSG and (b) proposed control.

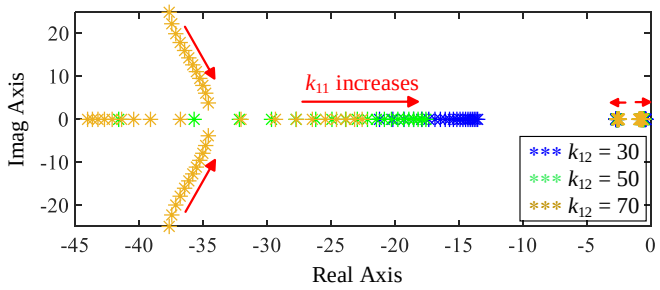

Fig. 9. Dominant poles of the proposed control when k_{11} increases from 1000 to 5000 with different k_{12}.

In the following, the matrix $\boldsymbol{A}_{new}$ is used to conduct a small-signal analysis. As the parallel VSGs have the same control structure as shown in Fig. 1, only the parameter variations of VSG1 is studied as an example and we only focus on the dominant poles. The required parameters are identical with the ones in the experiments given in Table I, which will be further described in Section IV in details.

For the purpose of comparison, Fig. 8(a) shows the loci of the traditional VSG when H_1 changes and Fig. 8(b) shows the result with the proposed control. It can be seen that when H_1 increases, all the three dominated poles of the traditional VSG move closer to the imaginary axis. The pair of plural poles can always influence the dynamics of the system. Moreover, from H_1 = 2 s, they have even larger impacts than the real pole. Thus, obvious oscillations will occur. Meanwhile, a small H_1 is not good for the frequency support. Fig. 8(b) shows that the proposed control can keep the dominant poles to be negative real, which implies a small oscillation.

Fig. 9 shows the root loci family, which is related to the parameters of the frequency feedback signal. As seen, when k_{12} is small (e.g., k_{12} = 30 or 50), all the dominant poles are negative real in the investigated range of k_{11}. In this situation, as k_{11} increases, one of the dominant poles move away from the imaginary axis with the others close to the imaginary axis. However, when k_{12} increases to 70 with a small k_{11}, a pair of plural poles will occur, which enlarges the oscillation of the system. This oscillatory mode can be canceled by further increasing k_{11}, which implies that the value of k_{11} should not be too small. Meanwhile, k_{12} is not supposed to be too small as well. As shown, the loci of a smaller k_{12} are closer to the imaginary axis, which will increase the settle time.

Then, the parameters of the frequency feedback should be chosen by making tradeoffs among the following principles:

1) In order to have a small settle time, the dominant negative real pole should be away from the imaginary axis with a certain distance (e.g., $\geq$ 0.5). Therefore, k_{11} should be small and k_{12} should be large;
2) In order to well damp the oscillation, the existing plural poles should be canceled. Therefore, k_{11} should be large;
3) In order to limit the high-frequency noise, the time constant of the frequency feedback should not be small (e.g., $\geq$ 0.01 s). Therefore, k_{12} should be small;

According to the upper principles, the desirable region of the parameters of the frequency feedback is shown in Fig. 10. In this paper, there is (k_{11}, k_{12}) = (3000, 50).

Fig. 11 shows the root loci family, which is related to the parameters of the power feedback signal. As seen, when k_{13} is small, there is a pair of plural poles with a small natural frequency, which is not preferable. As k_{13} increases, this pair of poles meet and are split into two negative real ones, which implies that the dominant oscillatory mode is canceled. However, if k_{14} is small (e.g., k_{14} = 30), one of the poles will meet another one to constitute a new pair of plural poles. Meanwhile, k_{14} is not supposed to be too large as well. This is because a large k_{14} will make the power feedback close to a differential term, which may amplify the noise.

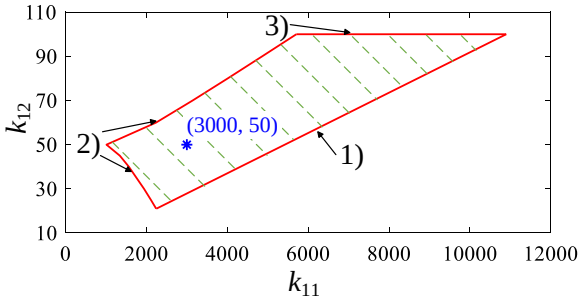

Fig. 10. Desirable region of parameters of frequency feedback, where 1), 2), and 3) means the boundaries are derived according to the corresponding principles.

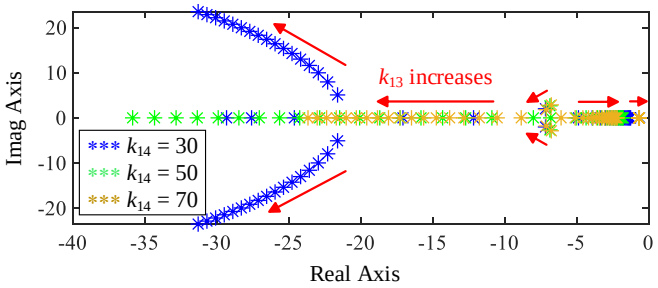

Fig. 11. Dominant poles of proposed control when k_{13} increases from 1 to 40 with different k_{14}.

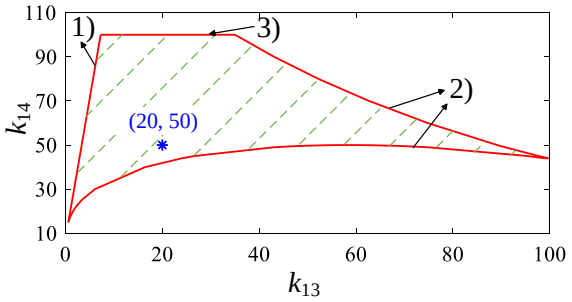

Fig. 12. Desirable region of parameters of power feedback, where 1), 2), and 3) means the boundaries are derived according to the corresponding principles.

Then, the parameters of the power feedback should be chosen by making tradeoffs between the following principles:

1) In order to well damp the oscillation, the existing plural poles should be canceled. Therefore, k_{13} and k_{14} should be large;
2) In order to avoid the introduction of new oscillation mode, there should be not new plural poles. Therefore, k_{13} should be small;
3) In order to limit the high-frequency noise, the time constant of the power feedback should not be small (e.g., $\geq$ 0.01 s). Therefore, k_{14} should be small;

According to the upper principles, the desirable region of the parameters of the power feedback is shown in Fig. 12. In this paper, there is (k_{13}, k_{14}) = (20, 50).

In conclusion, the parameters of the proposed controller should not be arbitrarily chosen. However, it is still feasible to design them in a relatively large range in order to damp the power oscillation.

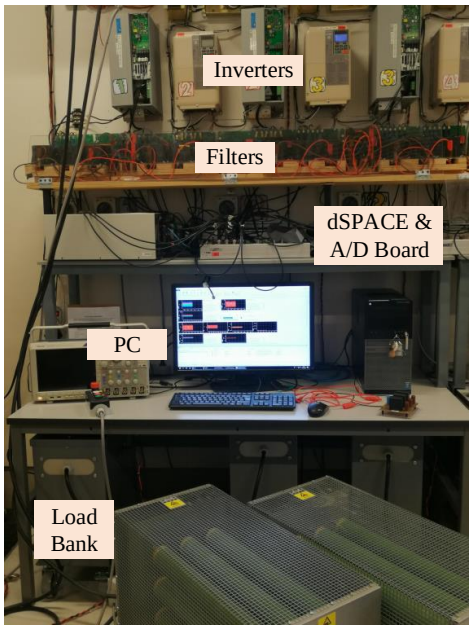

Fig. 13. Setup of experimental paralleled VSG system.

TABLE I
EXPERIMENTAL SETUP PARAMETERS

Parameter	Value	Parameter	Value
V_{dci}	700 V	P_{0i}	0.5 p.u.
L_{fi}	1.5 mH	ω_{0i}	100π rad/s
C_{fi}	20 μF	V_{0i}	1 p.u.
L_{si}	1 mH	Q_{0i}	0 p.u.
S_{ni}	5 kW	D_{p2}	0.02 p.u.
f_n	50 Hz	H_2	5 s
V_n	380 V	X_{v2}	1 Ω
f_{swi}	10 kHz	p^*_{load}	0.5 p.u.

IV. EXPERIMENTAL RESULTS

In order to verify the effectiveness of the proposed strategy, experimental tests are carried out on the setup shown in Fig. 13. The structure of the main circuit is identical with Fig. 2, where the inverter systems are based on Danfoss drives. The DS1007 dSPACE system is used to execute the control strategies. In order to demonstrate the effectiveness of the proposed control when the parameters of parallel VSGs do not meet a specific relationship like in [30] and [31], it is set that $D_{p1} = D_{p2}$, $H_1 = 2H_2$, and $X_{v1} = 3X_{v2}$. The other parameters are shown in Table I. When the system operates in steady-state, a load step of 0.5 p.u. is applied in order to study the dynamics.

With the set parameters, large oscillations are observed in the frequencies and output powers of the traditional VSGs as shown in Fig. 14(a). The peak value of p_1 is about 3400 W, which implies an oscillatory magnitude of 900 W. After about 1.5 s, the oscillation has been damped.

Fig. 14(b) shows the experimental results when only the power feedback signals are applied with the controller parameters given as $k_{13} = k_{23} = 20$ and $k_{14} = k_{24} = 50$. In this case, the oscillations with a smaller period can be damped

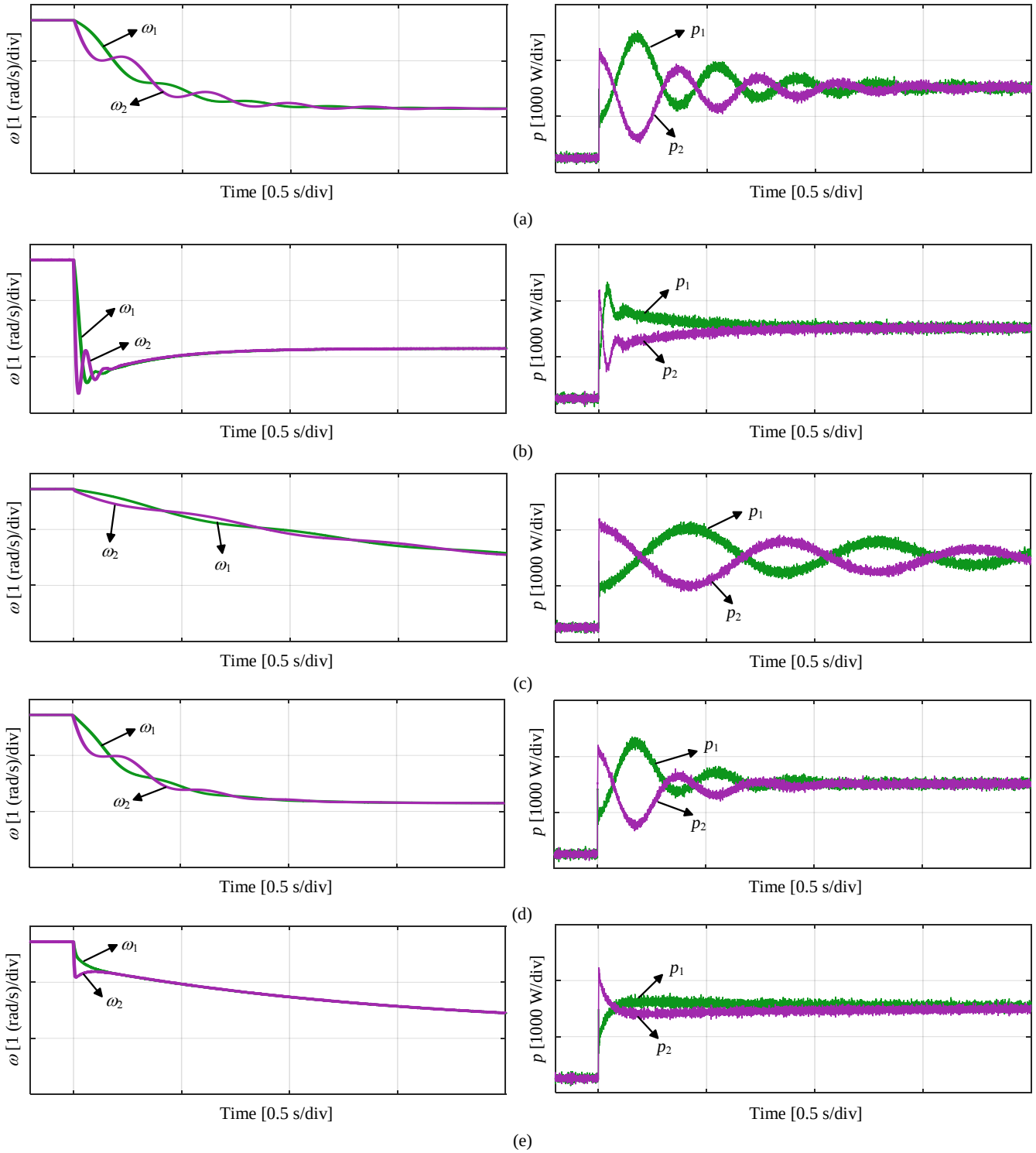

Fig. 14. Experimental results of frequency and active power with (a) traditional VSG (Case 1), (b) power feedback only (Case 2), (c) frequency feedback only (Case 3), (d) damping of $k_d(\omega^*\text{-}\omega_g)$, and (e) proposed control strategy.

less than 0.5 s, which is only 1/3 of the value in the traditional VSG case. However, the peak value is hardly decreased, which is 3200 W for p_1. Meanwhile, from the waveforms of the frequencies, they quickly drop to the values lower than the steady-state frequency after the disturbance. Therefore, this method seriously sacrifices the frequency quality compared with the methods in Fig. 14(a), Fig. 14(c), Fig. 14(d), and Fig. 14(e), which is not preferable.

When only the frequency feedback signals are applied by setting $k_{11} = k_{21} = 3000$ and $k_{12} = k_{22} = 50$, which is also the method in [31], the experimental results are as shown in Fig. 14(c). As it can be seen, although the oscillations can still be observed, the peak value of p_1 decreases to about 3000 W. Therefore, the oscillatory magnitude becomes 500 W, which

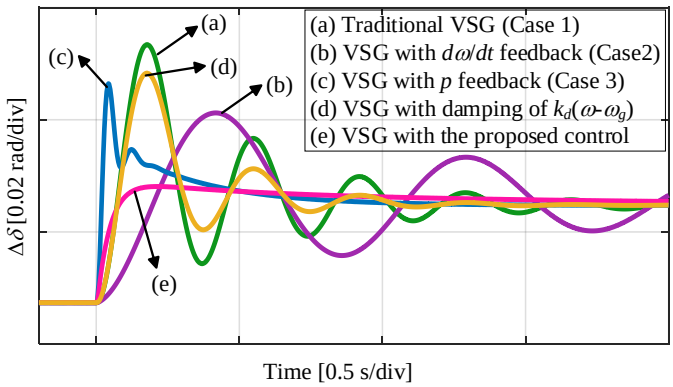

Fig. 15. Waveforms of relative rotor angle for different control methods.

is only 56% compared with the traditional VSG. However, the settling time increases due to a longer oscillation period. Fig. 14(c) shows that the oscillation can still be observed after 2 s, which is more than 1.3 times of the value in Fig. 14(a).

In order to better show the advantages of the proposed method, Fig. 14(d) presents the performance with the damping provided by $k_d(\omega^*\text{-}\omega_g)$, which is derived by a PLL or other equivalent forms in some literatures. The gain k_d is chosen to be identical with the frequency feedback gain of the proposed strategy. As analyzed in [30], it can only improve the damping but not eliminate the power oscillations if the parameters of the parallel VSGs do not meet a specific relationship.

Fig. 14(e) shows the experimental results with the proposed method, which feedbacks both the frequency and power signals. It is clearly shown that, compared with the traditional VSG and the methods with only frequency and power feedback signals, the oscillations in the frequencies and active powers can be well damped with just a small drop in the beginning of the dynamics of frequencies with the proposed method. It should also be noted that, although the controller parameters are set to be identical in the experiments, it is not a necessary condition as shown in Section III-C.

As the oscillations reflect the re-synchronization process between the parallel VSGs after a disturbance. Fig. 15 shows the relative rotor angle of VSG1 to VSG2. As it is seen, the re-synchronization process with the proposed control strategy is much smoother than the other four cases, which further verify the effectiveness of the proposed strategy.

V. Conclusion

In this paper, a new VSG control strategy is proposed in order to damp the power oscillations in a paralleled system. According to the analysis, the control targets can be transformed to a problem of controlling $d\omega/dt$ with the existence of disturbance. Then the proposed controller consists of an acceleration control achieved by a frequency feedback and a disturbance compensation achieved by a power feedback. The experimental results verify that the parallel VSGs can achieve quick re-synchronization following a load disturbance without causing large oscillation. It is also shown that the proposed strategy only use the local information rather than relying on a specific relationship between the parameters of the parallel VSGs. Therefore, a completely decentralized control method is achieved. However, the proposed method is only based on the small-signal analysis, which may not guarantee the effectiveness with a large disturbance.

References

[1] J. Rocabert, A. Luna, F. Blaabjerg, and P. Rodríguez, "Control of power converters in AC microgrids," *IEEE Trans. Power Electron.*, vol. 27, no. 11, pp. 4734–4749, Nov. 2012.
[2] J. Fang, H. Li, Y. Tang, and F. Blaabjerg, "Distributed power system virtual inertia implemented by grid-connected power converters," *IEEE Trans. Power Electron.*, vol. 33, no. 10, pp. 8488–8499, Oct. 2018.
[3] M. Chen and X. Xiao, "Hierarchical frequency control strategy of hybrid droop/VSG-based islanded microgrids," *Electr. Power Syst. Res.*, vol. 155, pp. 131–143, Feb. 2018.
[4] A. Fernández-Guillamón, E. Gómez-Lázaro, E. Muljadi, and Á. Molina-García, "Power systems with high renewable energy sources: A review of inertia and frequency control strategies over time," *Renew. Sustain. Energy Rev.*, vol. 115, pp. 1–12, Nov. 2019.
[5] Y. Wu, D. Zhang, L. Xiong, S. Wang, Z. Xu, and Y. Zhang, "Modeling and mechanism investigation of inertia and damping issues for grid-tied PV generation systems with droop control," *Energies*, vol. 12, no. 10, pp. 1–17, May 2019.
[6] S. A. Khajehoddin, M. Karimi-Ghartemani, and M. Ebrahimi, "Grid-supporting inverters with improved dynamics," *IEEE Trans. Ind. Electron.*, vol. 66, no. 5, pp. 3655–3667, May 2019.
[7] V. Natarajan and G. Weiss, "Synchronverters with better stability due to virtual inductors, virtual capacitors, and anti-windup," *IEEE Trans. Ind. Electron.*, vol. 64, no. 7, pp. 5994–6004, Jul. 2017.
[8] C. Li, Y. Li, Y. Cao, H. Zhu, C. Rehtanz, and U. Hager, "Virtual synchronous generator control for damping DC-side resonance of VSC-MTDC system," *IEEE J. Emerg. Sel. Top. Power Electron.*, vol. 6, no. 3, pp. 1054–1064, Sep. 2018.
[9] M. Chen, D. Zhou, and F. Blaabjerg, "Modelling, implementation, and assessment of virtual synchronous generator in power systems," *J. Mod. Power Syst. Clean Energy*, vol. 8, no. 3, pp. 399–411, May 2020.
[10] X. Meng, J. Liu, and Z. Liu, "A generalized droop control for grid-supporting inverter based on comparison between traditional droop control and virtual synchronous generator control," *IEEE Trans. Power Electron.*, vol. 34, no. 6, pp. 5416–5438, Jun. 2019.
[11] M. Ebrahimi, S. A. Khajehoddin, and M. Karimi-Ghartemani, "An improved damping method for virtual synchronous machines," *IEEE Trans. Sustain. Energy*, vol. 10, no. 3, pp. 1491–1500, Jul. 2019.
[12] J. Fang, H. Li, Y. Tang, and F. Blaabjerg, "On the inertia of future more-electronics power systems," *IEEE J. Emerg. Sel. Top. Power Electron.*, vol. 7, no. 4, pp. 2130–2146, Dec. 2019.
[13] J. Ying, X. Yuan, J. Hu, and W. He, "Impact of inertia control of DFIG-based WT on electromechanical oscillation damping of SG," *IEEE Trans. Power Syst.*, vol. 33, no. 3, pp. 3450–3459, May 2018.
[14] W. Du, Q. Fu, and H. F. Wang, "Power system small-signal angular stability affected by virtual synchronous generators," *IEEE Trans. Power Syst.*, vol. 34, no. 4, pp. 3209–3219, Jul. 2019.
[15] R. Rosso, S. Engelken, and M. Liserre, "Robust stability analysis of synchronverters operating in parallel," *IEEE Trans. Power Electron.*, vol. 34, no. 11, pp. 11 309–11 319, Nov. 2019.
[16] Z. Wang, F. Zhuo, H. Yi, J. Wu, F. Wang, and Z. Zeng, "Analysis of dynamic frequency performance among voltage-controlled inverters considering virtual inertia interaction in microgrid," *IEEE Trans. Ind. Appl.*, vol. 55, no. 4, pp. 4135–4144, Jul. 2019.
[17] M. Choopani, S. Hosseinain, and B. Vahidi, "A novel comprehensive method to enhance stability of multi-vsg grids," *Int. J. Electr. Power Energy Syst.*, vol. 104, pp. 502–514, Jan. 2019.
[18] K. Shi, W. Song, H. Ge, P. Xu, Y. Yang, and F. Blaabjerg, "Transient analysis of microgrids with parallel synchronous generators and virtual synchronous generators," *IEEE Trans. Energy Convers.*, vol. 35, no. 1, pp. 95–105, Mar. 2020.
[19] L. Huang, H. Xin, and Z. Wang, "Damping low-frequency oscillations through VSC-HVdc stations operated as virtual synchronous machines," *IEEE Trans. Power Electron.*, vol. 34, no. 6, pp. 5803–5818, Jun. 2019.
[20] Y. Wang, J. Meng, X. Zhang, and L. Xu, "Control of PMSG-based wind turbines for system inertial response and power oscillation damping," *IEEE Trans. Sustain. Energy*, vol. 6, no. 2, pp. 565–574, Apr. 2015.
[21] J. Chen and T. O'Donnell, "Parameter constraints for virtual synchronous generator considering stability," *IEEE Trans. Power Syst.*, vol. 34, no. 3, pp. 2479–2481, May 2019.

[22] M. Ashabani and Y. A.-R. I. Mohamed, "Integrating VSCs to weak grids by nonlinear power damping controller with self-synchronization capability," *IEEE Trans. Power Syst.*, vol. 29, no. 2, pp. 805–814, Mar. 2014.
[23] T. Shintai, Y. Miura, and T. Ise, "Oscillation damping of a distributed generator using a virtual synchronous generator," *IEEE Trans. Power Deliv.*, vol. 29, no. 2, pp. 668–676, Apr. 2014.
[24] J. Alipoor, Y. Miura, and T. Ise, "Power system stabilization using virtual synchronous generator with alternating moment of inertia," *IEEE J. Emerg. Sel. Top. Power Electron.*, vol. 3, no. 2, pp. 451–458, Jun. 2015.
[25] D. Li, Q. Zhu, S. Lin, and X. Y. Bian, "A self-adaptive inertia and damping combination control of VSG to support frequency stability," *IEEE Trans. Energy Convers.*, vol. 32, no. 1, pp. 397–398, Mar. 2017.
[26] X. Zhang, F. Mao, H. Xu, F. Liu, and M. Li, "An optimal coordination control strategy of micro-grid inverter and energy storage based on variable virtual inertia and damping of vsg," *Chinese J. Electr. Eng.*, vol. 3, no. 3, pp. 25–33, Dec. 2017.
[27] S. Dong and Y. C. Chen, "Adjusting synchronverter dynamic response speed via damping correction loop," *IEEE Trans. Energy Convers.*, vol. 32, no. 2, pp. 608–619, Jun. 2017.
[28] A. Adib and B. Mirafzal, "Virtual inductance for stable operation of grid-interactive voltage source inverters," *IEEE Trans. Ind. Electron.*, vol. 66, no. 8, pp. 6002–6011, Aug. 2019.
[29] A. Rodriguez-Cabero, J. Roldan-Perez, and M. Prodanovic, "Virtual impedance design considerations for virtual synchronous machines in weak grids," *IEEE J. Emerg. Sel. Top. Power Electron.*, vol. 8, no. 2, pp. 1477–1489, Jun. 2020.
[30] J. Liu, Y. Miura, H. Bevrani, and T. Ise, "Enhanced virtual synchronous generator control for parallel inverters in microgrids," *IEEE Trans. Smart Grid*, vol. 8, no. 5, pp. 2268–2277, Sep. 2017.
[31] Z. Shuai, W. Huang, Z. J. Shen, A. Luo, and Z. Tian, "Active power oscillation and suppression techniques between two parallel synchronverters during load fluctuations," *IEEE Trans. Power Electron.*, vol. 35, no. 4, pp. 4127–4142, Apr. 2020.
[32] R. C. Dorf and R. H. Bishop, *Modern Control Systems*. Prentice Hall, 2010.
[33] N. Pogaku, M. Prodanovic, and T. C. Green, "Modeling, analysis and testing of autonomous operation of an inverter-based microgrid," *IEEE Trans. Power Electron.*, vol. 22, no. 2, pp. 613–625, Mar. 2007.